Applied Catalysis B: Environmental 140–141 (2013) 588–597

Contents lists available at SciVerse ScienceDirect

Applied Catalysis B: Environmental

journal homepage: www.elsevier.com/locate/apcatb

Preparation, characterization and application of K-PtCo/Al_2O_3 catalyst coatings for preferential CO oxidation

Xinhai Yu[a,b,*], Wei Yu[a], Hongliang Li[a], Shan-Tung Tu[a], Yi-Fan Han[c]

[a] Key Laboratory of Pressure Systems and Safety (MOE), School of Mechanical and Power Engineering, East China University of Science and Technology, Shanghai, 200237, China
[b] State Key Laboratory of Bioreactor Engineering, East China University of Science and Technology, Shanghai, 200237, China
[c] State Key Laboratory of Chemical Engineering, East China University of Science and Technology, Shanghai, 200237, China

ARTICLE INFO

Article history:
Received 28 July 2012
Received in revised form 24 March 2013
Accepted 30 April 2013
Available online 7 May 2013

Keywords:
Preferential CO oxidation
Catalyst coating
Bimetallic PtCo catalysts
Micro-reactor
Hydrogen purification

ABSTRACT

K-PtCo/Al_2O_3 catalyst coatings were studied concerning preferential oxidation of carbon monoxide (PROX) in hydrogen-rich gas streams. It has been found that the addition of potassium can enhance the catalytic activities at temperatures below 413 K, thus can widen the window of operation in terms of reaction temperatures. The most active catalyst coating of 1.5K-Pt2Co (Pt 1 wt.%, Co 2 wt.%, and K/Co molar ratio of 1.5) can reduce carbon monoxide concentrations from initial 1% to less than 10 ppm at a high *GHSV* of 120,000 ml g^{-1} h^{-1} in a temperature range 393–433 K. The structure of catalyst coatings has been thoroughly characterized using multi-techniques, such as high-resolution transmission electron microscopy (HRTEM), X-ray photoelectron spectroscopy (XPS), temperature programmed reduction (TPR), *in situ* laser Raman spectroscopy and *in situ* diffuse reflectance infrared Fourier transform spectroscopy (*in situ* DRIFTS). The addition of K has evidenced to promote the formation of Pt_3Co and increase the particle size as identified by TEM and XPS. Pt_3Co plays an important role in PROX. For PtCo/Al_2O_3 catalyst coatings, a redox equilibrium for Co during PROX was found. In contrast, with the addition of K, this redox equilibrium disappeared, probably because of the increased amount of Pt_3Co phase in the catalyst surface region.

1. Introduction

Proton exchange membrane fuel cells (PEMFC) and phosphoric acid fuel cells (PAFC) have been studied extensively in recent years, showing considerable promise for both stationary and automotive power supply. These fuel cells typically use the electrochemical reaction between hydrogen, as the fuel, and air or oxygen, as the oxidant. The hydrogen fuel produced by reforming of organic molecules such as alcohols [1] generally contains low levels of CO as an impurity. For PEMFC, ultralow levels of CO in hydrogen fuel (commonly below 10 ppm) are mandatory in order to prevent the poisoning of the Pt-based PEMFC's catalysts [2]. The water-gas shift reaction (Eq. (1))

$$CO + H_2O = CO_2 + H_2 \quad \Delta H_{298^\circ} = -283.6\,\text{kJ mol}^{-1} \tag{1}$$

is considered as the first cleaning step, which can only reduce the CO contents to 0.5–1% CO [3]. Further reducing CO to 10 ppm is still a challenge for fuel cell application. Several methods have been developed for the removal of CO from H_2-rich streams in the last decades, including cryogenic separation, pressure swing adsorption, selective diffusion, CO selective methanation (CO-SMET) [4], and preferential oxidation of CO (PROX) (Eq. (2), avoiding oxidation of hydrogen as shown in Eq. (3)).

$$CO + \tfrac{1}{2}O_2 = CO_2 \quad \Delta H_{298^\circ} = -283.6\,\text{kJ mol}^{-1} \tag{2}$$

$$H_2 + \tfrac{1}{2}O_2 = H_2O \quad \Delta H_{298^\circ} = -243.5\,\text{kJ mol}^{-1} \tag{3}$$

In general, in order to reduce the loss of energy efficiency, the consumption of H_2 should be avoided when removing CO. Comparatively, among the listed methods of CO removal, CO-SMET and PROX are effective and feasible methods for the development of practical applications [5,6].

The development of catalysts with higher activity and selectivity is always the most important technique for the PROX reaction. Supported noble metals, such as Pt [7], Pd [8], Ru [9], Au [10], Rh [11], and Sn [12], have been evaluated. Pt-based bimetallic catalysts prepared by adding other metals, such as Co [13], Nb [14], Ce [15], Au [16], and Sn [17], have found to be promising candidates.

The PROX reaction is usually carried out in a fixed-bed reactor, which has a number of inherent problems, such as hot and cold spots as well as a poor response to transients. Comparatively,

* Corresponding author at: Meilong Road 130, 200237, Shanghai, China. Tel.: +86 21 64253513; fax: +86 21 64253513.
E-mail address: yxhh@ecust.edu.cn (X. Yu).

0926-3373/$ – see front matter © 2013 Elsevier B.V. All rights reserved.
http://dx.doi.org/10.1016/j.apcatb.2013.04.066

straight-channel monolith reactors with thin-film catalyst coatings have proved to enhance the diffusion of reactants toward the active sites and they show low heat capacity, which provides rapid responses to changes in the operating conditions of fuel cells [18]. Micro-channel reactors with catalyst coatings show negligible external and internal mass transport limitations as well as enhanced heat transport characteristics. So, these reactors have advantages, such as rapid heating and cooling, suppression of hot spots, fast response rates, and easy integration with miniaturized devices [19]. Likely, with the concerns of intrinsic safety and scale up, micro-structure reactors are ideally suited for PROX when coupled with PEMFC systems in low- to medium-power output applications [20,21].

The properties of the catalyst coatings are crucial to monolith and micro-channel reactors. However, studies about the catalyst coatings for PROX is limited [22–27]. As far as most of the reported catalyst coatings are concerned, an outlet CO concentration of less than 10 ppm was obtained at high temperatures (>460 K) for PROX. Therefore, deep insight into catalyst coatings for PROX is highly desired.

One of our previous studies has reported that a Pt-Co/Al_2O_3 catalyst coating was active for PROX by decreasing CO concentration to less than 10 ppm in a simulated reformate gas containing H_2O and CO_2, which was attributed to the formation of Pt_3Co intermetallic compounds [28]. In addition, the promotional effects of alkali metals on Pt-based powdered catalysts have been studied for this reaction. Masatoshi et al. [29] reported that a K-Pt/Al_2O_3 powdered catalyst was very active in the PROX reaction because the potassium weakened the interaction between CO and Pt by changing the adsorption sites. Kwak et al. [30] found that the addition of sodium to powdered Pt-Co/Al_2O_3 catalysts could promote the formation of Pt-Co bimetallic phases and improve the catalytic performance. To our best knowledge, few works were reported for the Pt-Co catalyst coatings promoted by alkali metals for PROX; in particular, the structure of active sites for Pt-Co catalysts upon the addition of alkali metals and corresponding catalytic mechanisms are still unclear.

In this paper, we investigate the preparation of an active K-PtCo/Al_2O_3 catalyst coating, and the PROX reaction was carried out using an annular micro-reactor. The catalyst composition for PROX in H_2-rich gas streams was optimized. To understand the role of K, the origins of active sites were studied using a combination of techniques, including high-resolution transmission electron microscopy (HRTEM), *in situ* laser Raman spectroscopy (LRS), X-ray photoelectron spectroscopy (XPS), temperature programmed reduction (TPR), and *in situ* diffuse-reflectance infrared Fourier transform spectroscopy (*in situ* DRIFTS). The aim of the present study was to examine the effect of K addition into the PtCo/Al_2O_3 catalyst coatings and to develop a substantive method to prepare an active catalyst coating with low Pt loading.

2. Experimental

2.1. Catalyst coating preparation

The catalyst coatings were prepared using an impregnation method [31]. Briefly, a γ-Al_2O_3 powder (home made) with a surface area of 248 $m^2\,g^{-1}$ was ball-milled for 24 h and slowly added into a stirred solution of nitric acid, chloroplatinic acid hexahydrate, cobalt nitrate and potassium nitrate. The slurry was stirred for 2 h, left to stand for 2 h, and coated on a Fe-Cr-Al alloy cylinder. The catalyst coatings were air-dried and calcined at 773 K for 2 h. It should be noted that the Pt, Co and K loadings were identified with controlling the concentration of chloroplatinic acid hexahydrate, cobalt nitrate and potassium nitrate. Catalyst coatings prepared by this impregnation method are hereafter denoted as (*a*) k-(*b*)Pt(*c*)Co, where *a* is the molar ratio of K to Pt. The *b* and *c* are the Pt and Co loadings in wt.%, respectively. The real metal loading of the samples is very close to the nominal value as measured by inductively coupled plasma (ICP).

2.2. Catalytic measurements

The activity measurements were carried out using an annular micro-reactor consisting of an internal cylinder coaxially placed in an external tube. The catalyst was deposited on the walls of the annular micro-reactor. The details of this set-up can be seen in a previous study [28]. Before the reaction, the catalyst was pretreated with water at a flow rate of 0.25 ml min^{-1} using a syringe pump under a H_2 flow at 673 K for 2 h. Then, the temperature was gradually decreased to a reaction temperature under a He flow. The feed gas contains 50% H_2, 20% CO_2, 1% O_2, 1% CO, 16% H_2O, 0.5% CH_4 and He as a balance gas.

The effluent of the reactor consisted of H_2, CO_2, CO, He, CH_4, and H_2O, which was removed from the exit gas by passing the stream through a cold trap. An online gas chromatography (GC) with a thermal conductivity detector (TCD) was used to measure the inlet and outlet O_2 concentrations, and a flame ionization detector (FID) was used to determine the concentration of CO, CH_4, and CO_2. A molecular sieve (5A) column was used to separate He, O_2, CH_4, and CO, and a TDX column was used to isolate CO_2. After the column, a converter was used to convert CO or CO_2 to CH_4. The minimum detection level for CO and CO_2 was 1 ppm. CO_2 selectivity is defined as the ratio of O_2 consumption for CO oxidation over the total O_2 consumption.

2.3. Catalyst characterization

N_2 adsorption–desorption measurements were performed using a Micrometrics Tristar 3000 apparatus. Prior to measurement, the samples were degassed under a vacuum at 573 K for 24 h. The specific surface area was determined using the multipoint Brunauer–Emmett–Teller (BET) method. The pore volume and pore size distribution were calculated according to the Barrett–Joyner–Halenda (BJH) method.

The TEM and HRTEM images were obtained at room temperature on a JEM 2100F (UHR), which was operated at an accelerating voltage of 200 kV. For qualitative analysis, selected-area electron diffraction (SAED) patterns were obtained from specimen areas using scanning transmission electron microscopy (STEM) images of approximately 100 nm. The samples were prepared by dipping a Cu-grid (made of an ultrathin pure carbon-support film with no formvar backing) into a sonicated dispersion of the sample in deionized water. The average particle size was estimated from a statistical result of 100 particles randomly selected in the TEM images.

The XPS measurements were performed using a Thermo ESCALAB 250 spectrometer. A monochromatic Al Kα radiation source ($h\nu$ = 1486.6 eV) was used at a spot size of 500 μm. The analyzer was in constant resolution mode and used a pass energy of 20 eV. The full width at half maximum (FWHM) of the Ag $3d_{5/2}$ peak at 0.6 eV was determined using a clean silver specimen. The energy scale was internally calibrated by setting the Al 2p peak to 74.4 eV. Prior to curve fitting, X-ray satellites and inelastic backgrounds (Sherwood-type) were subtracted. A Gaussian of 80% and a Lorentzian peak of 20% were used for peak deconvolution.

In situ Raman spectra were obtained using a confocal Raman microscope (Renishaw inVia microscope). The Raman scattering of the samples in an *in situ* cell (Linkam, THMS600) were excited using an argon (Ar) ion laser (514 nm). The spectra were collected with a 1 cm^{-1} spectral resolution (1800 lines/mm grating). The cell

ensured homogenous temperature distribution with a precision of 0.1 K. Each sample was placed at the bottom of the cell and exposed to the gases introduced at the cell inlet. The spectrum acquisition time for each sample was 30 s.

TPR was performed using a Micromeritics AutoChem II 2920 automated catalyst characterization system. A sample of 100 mg was loaded into a U-shaped quartz reactor and pre-treated in Ar at 573 K for 1 h. After cooling to room temperature, the flow gas was switched to 10-vol% H_2/Ar, and the catalyst was heated to 1173 K at a rate of 10 K min^{-1}. Effluent gas was dried by powder KOH and the consumption of hydrogen were recorded by thermal conductivity detector (TCD). Calibration of the instrument was carried out with CuO of known amount.

The formation of adsorbents on the samples was followed by *in situ* FTIR spectroscopy in smart diffuse reflectance mode with a PerkinElmer FT-IR spectrum 100 spectrometer equipped with a liquid nitrogen-cooled mercury-cadmium-telluride (MCT) detector (resolution: 4 cm^{-1}) and a reaction chamber (modified Harricks HV-DR2 model) with a zinc–selenium (Zn–Se) window. All infrared data were evaluated in Kubelka–Munk units, which are linearly related to the absorber concentration in the spectra. The catalyst sample of 30 mg powder was pretreated *in situ* according to the activation procedure described in Section 2.2. For CO absorption measurements, after pretreatment, background spectra were collected at 313 K in He. The samples were subsequently saturated with CO in a 2% CO flow. The spectra were recorded after blowing He at 313 K over the samples for 20 min. For *In situ* DRIFT spectra measurements, after pretreatment, the samples were cooled to 433 K under a high-purity He flow. Then, the background spectra were collected at 433 K in He. The samples were subsequently exposed to reactant gases (1% CO, 1% O_2, 1% CO_2, 48% H_2, and He), and the spectra were recorded with the evolution of the PROX reaction.

The catalyst coating powder samples tested using HRTEM, XPS, *in situ* laser Raman spectroscopy and *in situ* DRIFTS measurements were scraped from the Fe–Cr–Al alloy cylinder support.

3. Results and discussion

3.1. Catalytic testing for PROX in an annular micro-reactor

3.1.1. Effect of K

Catalytic activity was performed at 393, 433 and 473 K, respectively. The CO outlet concentration as a function of the K/Pt molar ratio is presented in Fig. 1. The O_2 concentration in the feed gas for PROX is usually in the range of 1–2%, as presented in Table 1. It is well known that a high O_2 concentration is favorable for PROX. For the catalyst coatings, a big difference in CO conversion is helpful to explain the effect of K concentration on the catalytic activity. The big difference is easy to be obtained at a low CO conversion, thus suggesting that a low O_2 concentration should be taken. Therefore, the O_2 concentration was set as 1% in this case. At 393 K, the CO conversion increased from 82.3% to 98.9% with an increase in the K/Pt molar ratio from 0 to 1.5 and decreased to 87.5% after a maximum of 98.9%. Similar trends of CO conversion at 433 and 473 K were observed with the respective maximal values of 99.9% and 93.4% at a K/Pt molar ratio of 1.5. Therefore, the optimum K/Pt molar ratio of catalyst is about 1.5, being denoted as 1.5K-Pt2Co. The reason for the decrease in CO conversion when the K/Pt molar ratio exceeds 1.5 is discussed in section 3.2. The catalyst coating of 1.5K-Pt was prepared under exactly the same conditions as described in section 2.1. Fig. 2 shows the effects of reaction temperature on CO conversion in PROX reaction for Pt2Co, 1.5K-Pt2Co and 1.5K-Pt2Co. The highest CO conversion was achieved for 1.5K-Pt2Co within 393–473 K. The catalyst of 1.5K-Pt showed the lowest CO conversion within 393–453 K. At 473 K, the CO conversion of 1.5K-Pt was higher than that of Pt2Co.

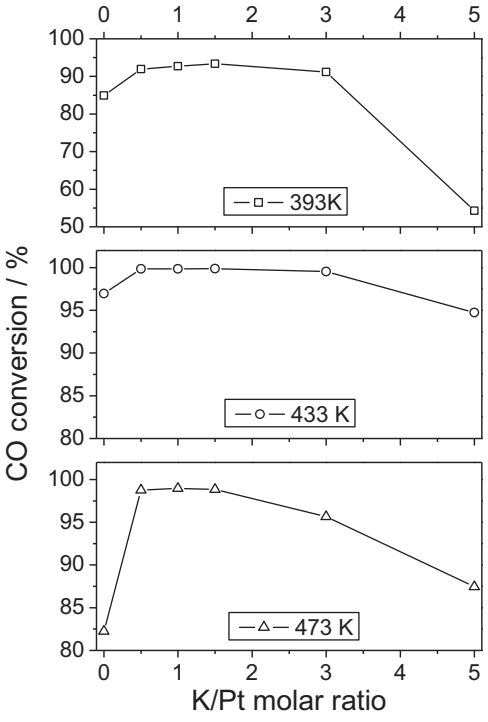

Fig. 1. Effect of the molar ratio of K/Pt on CO conversion in PROX reaction (50% H_2, 1% CO, 1% O_2, He, and *GHSV* of 80000 ml g^{-1} h^{-1}).

3.1.2. Performance of 1.5K-Pt2Co

We investigated the PROX on the 1.5K-Pt2Co catalyst coating in a simulated reformate gas (50% H_2, 1.5% O_2, 1% CO_2, 16% H_2O, and He). It should be noted that the lowest O_2 consumption rate is not a mandatory issue when compared to the need for avoiding PEMFC electrocatalyst poisoning by CO. This is a very important issue, especially for a reactor that is part of a fuel processor onboard a vehicle. This reactor should be easily controllable to assure complete CO removal, which suggests that the reactor working temperature should be in a sufficiently wide range for complete CO abatement. Therefore, the inlet O_2 concentration was increased from 1% to 1.5% to achieve a wide working temperature. As illustrated in Fig. 3,

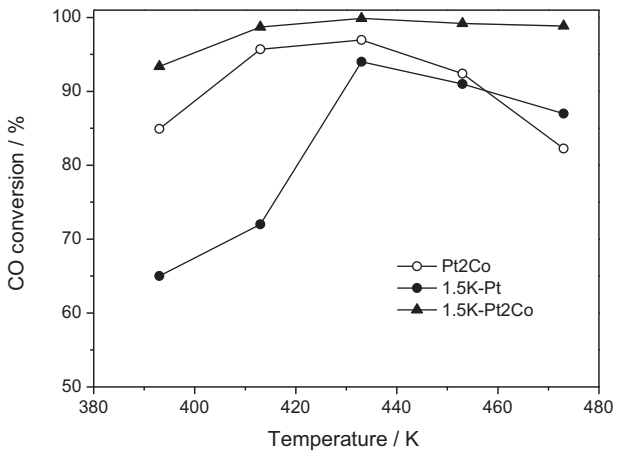

Fig. 2. Effect of reaction temperature on CO conversion in PROX reaction for Pt2Co, 1.5 K-Pt2Co and 1.5 K-Pt2Co (50% H_2, 1% CO, 1% O_2, He, and *GHSV* of 80,000 ml g^{-1} h^{-1}).

Table 1
Comparison of the catalytic performance of catalyst coatings for PROX reported in the literature and obtained in the present work.

Catalyst	Reactor structure	Feed		Temperature (K)	Exit CO concentration (ppm)	GHSV	Stability	Reference
		O_2	CO					
5.0 wt% Pt/Al_2O_3	Silicon-based multi-channeled micro-reactor	2%	1%	533	60	217,390 h^{-1}	Not mentioned	[22]
2.0 wt% $Rh\text{-}K/Al_2O_3$	Stainless steel microchannel reactor	1%	1%	450–493	50	100,000 h^{-1}	Not stable	[23]
1.0 wt% $Pt\text{-}MIX/Al_2O_3$	Metal plate-channels reactor	2%	0.5%	467–487 488–498	2	2000 h^{-1} 4800 h^{-1}	Not mentioned	[24]
5.0 wt% Cu/CeO_{2-x}	Stainless steel microchannel reactor	1.5%	1%	463–513	10	55,000 ml g^{-1} h^{-1}	Not mentioned	[25]
4.0 wt% Pt-0.5 wt% Fe/mordenite	Ceramic straight-channel monoliths reactor	1%	1%	403	10	5800–9500 h^{-1}	Stable	[26]
5.0 wt% $Pt\text{-}4.5\%\ Co/Al_2O_3$	Multi-layered micro-reactor	2%	0.8%	~423	50	Not mentioned	Not mentioned	[27]
1.0 wt% $Pt\text{-}2\ wt\%\ Co/Al_2O_3$	Annular micro-reactor	1.5%	1%	393–423 413–433	1–10	40,000 ml g^{-1} h^{-1} 120,000 ml g^{-1} h^{-1}	Stable	[28]
1.5 wt% K-1 wt% $Pt\text{-}2\ wt\%\ Co/Al_2O_3$	Annular micro-reactor	1.5%	1%	393–433	1–10	120,000 ml g^{-1} h^{-1}	Stable	Present work

a temperature range of 40 K (393–433 K) was achieved for 1.5K-Pt2Co with CO outlet concentrations of 1–10 ppm. For Pt2Co, at the same *GHSV* of 120,000 ml g^{-1} h^{-1}, the low outlet CO concentration (1–10 ppm) was achieved at 413–433 K. Thus, the addition of potassium can enhance the catalytic activity at low temperatures and widen the reaction-temperature window of operation. For the PROX reaction, this is crucial to reducing the energy consumption and improving operational flexibility.

The stability of the 1.5K-Pt2Co catalyst was continuously operated for 100 h, as a long-term durability of 10 years is required for residential PEMFC systems [32] at 413 K with *GHSV* of 120,000 ml g^{-1} h^{-1}. As the feed of the PROX unit of a practical fuel processor (FP) has CH_4 regardless of which hydrocarbon/hydrocarbon mixture is fed to the reformer unit of the FP, the stability test was carried out using a feed mixture including CH_4. The concentration of CH_4 was chosen as 0.5% in accordance with the experimental results by Suetsuna et al. who conducted steam reforming of methanol with the steam/methanol ratio of 4 using Cu-Ni based catalysts [33]. The stream composition was set as 50% H_2, 1.5% O_2, 1% CO_2, 16% H_2O, 0.5% CH_4 and He. As depicted in Fig. 4, an initial activation occurred within the first 1 h of operation. The outlet CO concentration and CO_2 selectivity stabilized at a level below 10 ppm and approximately 40%, respectively, for a *GHSV* of 120,000 ml g^{-1} h^{-1}. Although a longer-term durability test is still essential for the practical application, we believe that the stability observed in this study demonstrates the high potential of this catalyst as a practical catalyst coating for a PROX reactor. In addition, the CH_4 concentration at the reactor outlet kept 0.5%, suggesting that 1.5K-Pt2Co is not active for CH_4 conversion.

Table 1 lists the performances of the catalyst coatings for PROX from the recent literature and this study. Compared with other catalyst coatings, an excellent performance of 1.5K-Pt2Co can be clearly observed. The catalyst coating used in the present work only contains 1.0 wt.% Pt, and the fabrication cost is remarkably reduced. In addition, the catalyst coating of 1.5K-Pt2Co is able to function under a wide window of operation for temperature and at lower temperatures, indicating easy reaction control and lower energy consumption in its application.

3.2. Catalyst characterization

3.2.1. TEM and HRTEM

The morphology and structural details of the catalyst coatings after PROX reaction were examined using TEM to ascertain their crystalline and particle sizes. Crystals of Pt and Co are expected to yield highly contrasted and morphologically resolved images compared to the faintly contrasted images of poorly crystallized grains of alumina [34]. Figs. 5a and 6a show the morphologies and primary particle sizes of Pt2Co and 1.5K-Pt2Co catalysts against a bright field. A considerable uniformity of catalyst particles was

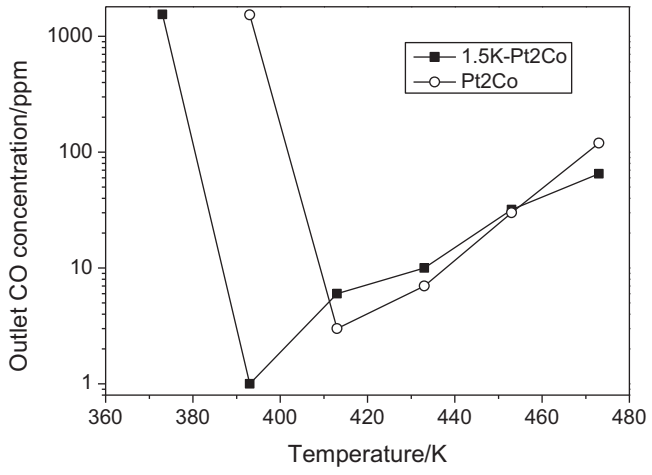

Fig. 3. The outlet concentrations of carbon monoxide as functions of reaction temperatures for 1.5K-Pt2Co and Pt2Co. The gas feed contained 1% CO, 1.5% O_2, 20% CO_2, 16% H_2O, 50% H_2, and He. *GHSV* = 120,000 ml g^{-1} h^{-1}.

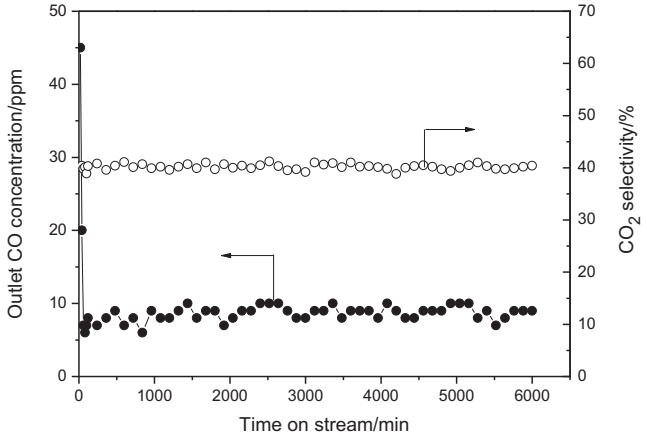

Fig. 4. Effect of the reaction time on the performance of 1.5K-Pt2Co at 413 K (1% CO, 1.5% O_2, 20% CO_2, 16% H_2O, 50% H_2, 0.5% CH_4, and He. *GHSV* = 120,000 ml g^{-1} h^{-1}).

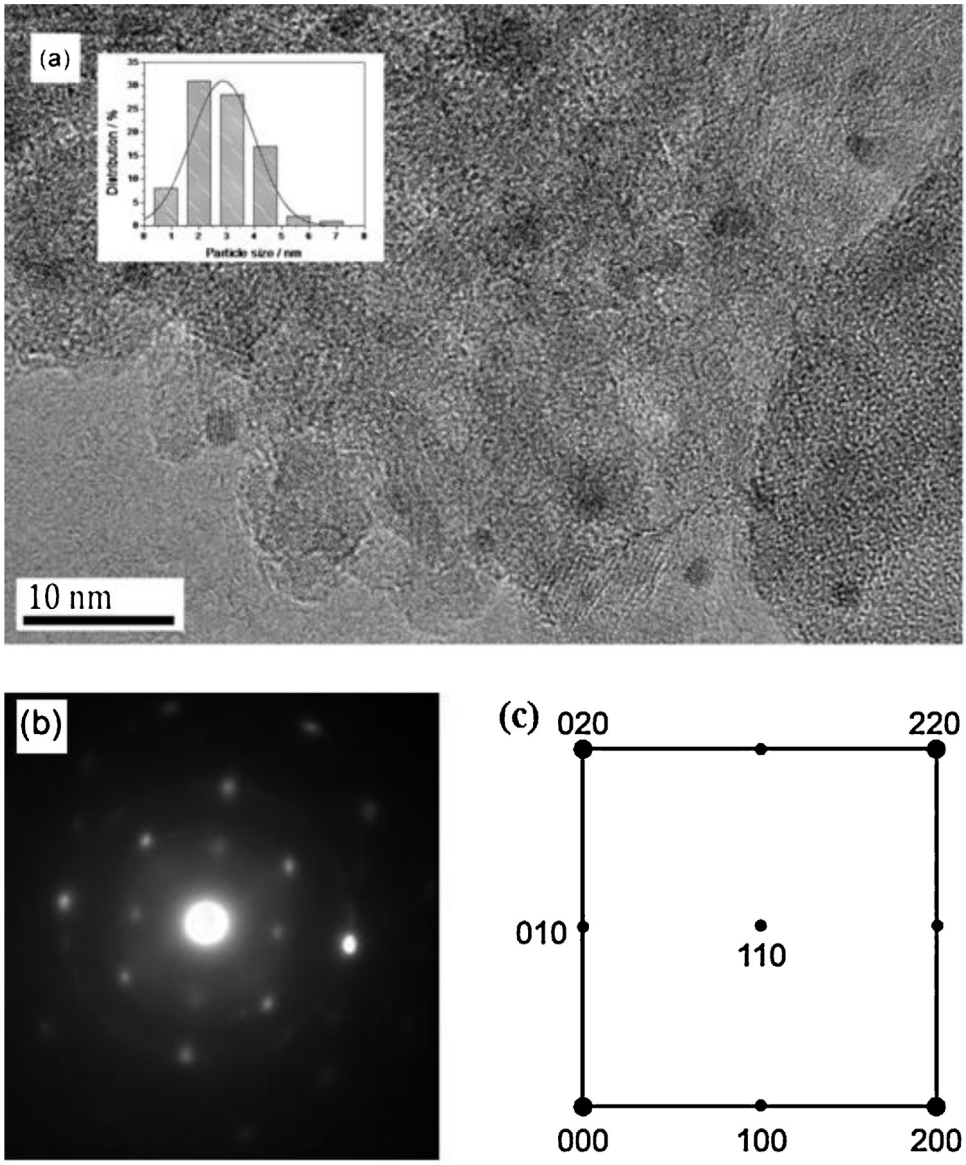

Fig. 5. TEM images and SAED pattern of Pt2Co: (a) TEM image with inset particle size distribution against a bright field; (b) SAED pattern in the [0 0 1] lattice direction; (c) enlarged representation of superlattice reflections.

observed for all catalyst coatings. These well-contrasted particles, presumably Pt, Pt-Co alloy, potassium oxides or CoO_x species, were scattered on the surface of the lightly contrasted matrix. The corresponding particle-size distributions are presented as insets. The miniscule metal particles were obtained, and the size of the contrasted particles, measured from a number of TEM micrographs, ranged from 2 to 8 nm. The average particle size of 1.5K-Pt2Co catalysts was 4.9 nm, which is 1.75 times that of the Pt2Co sample (2.8 nm). This tendency of the increase of particle size due to the addition of potassium is consistent with that of K-Pt/Al_2O_3 catalysts reported by Kuriyama et al. [29]. A considerable increase in particle size is unfavorable for PROX. However, in this case, 1.5K-Pt2Co exhibited higher catalytic activity than Pt2Co, which might be related to the modification of the local chemical environment with the addition of potassium.

The nature of these putative changes was analyzed with SAED and HRTEM. For Pt2Co, lattice fringes were difficult to be observed using HRTEM. The SAED measurements were therefore conducted to clarify the crystalline structures. The SAED pattern for the region shown in Fig. 5a is presented in Fig. 5b with its schematics (Fig. 5c). As shown in Fig. 5b, superlattice reflections are clearly evidenced, indicating the formation of the Pt_3Co intermetallic compound. The related details were reported in our previous study [28]. For 1.5K-Pt2Co, sharp and clear lattice fringes were detected in the HRTEM images (Fig. 6b), indicating good crystalline perfection. The values of interplanar spacing (d) were determined as 0.222 nm and 0.192 nm, corresponding to the standard d values for the (1 1 1) and (2 0 0) planes of the Pt_3Co phase (JCPDS 29-0499). Therefore, the Pt_3Co intermetallic compound was definitely generated when potassium was added in this case.

3.2.2. *In situ* laser Raman spectroscopy

Fig. 7 shows *in situ* Raman spectra for Pt2Co and 1.5K-Pt2Co. The alumina component exhibited no Raman reflection signal because alumina is not Raman active [35]. Vuumam et al. reported that the Raman spectra of CoO exhibit weak bands at *ca.* 680, 600 and 475 cm^{-1} with 514.5 nm excitation [36]. Liorca et al. assigned the bands at 674, 607, 512, 469 cm^{-1} to Co_3O_4 [37]. Hadjiev et al. reported the bands at 691, 618, 522, 482 cm^{-1} for single-crystal Co_3O_4 [38]. Before pretreatment at 673 K, four bands at 674, 615,

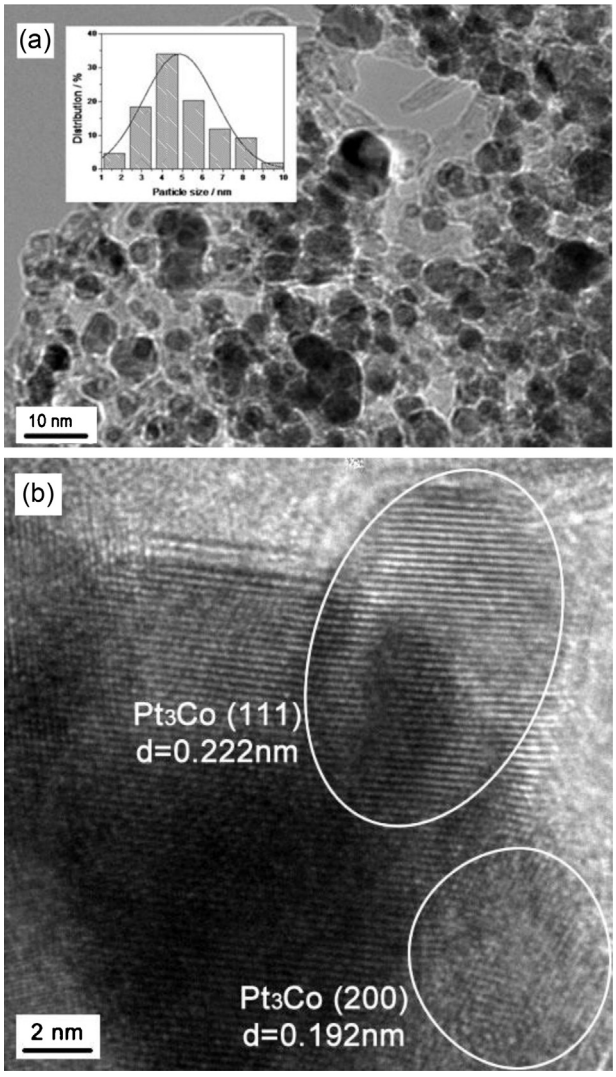

Fig. 6. TEM and HRTEM images of 1.5K-Pt2Co: (a) TEM image with inset particle size distribution against a bright field (b) HRTEM image.

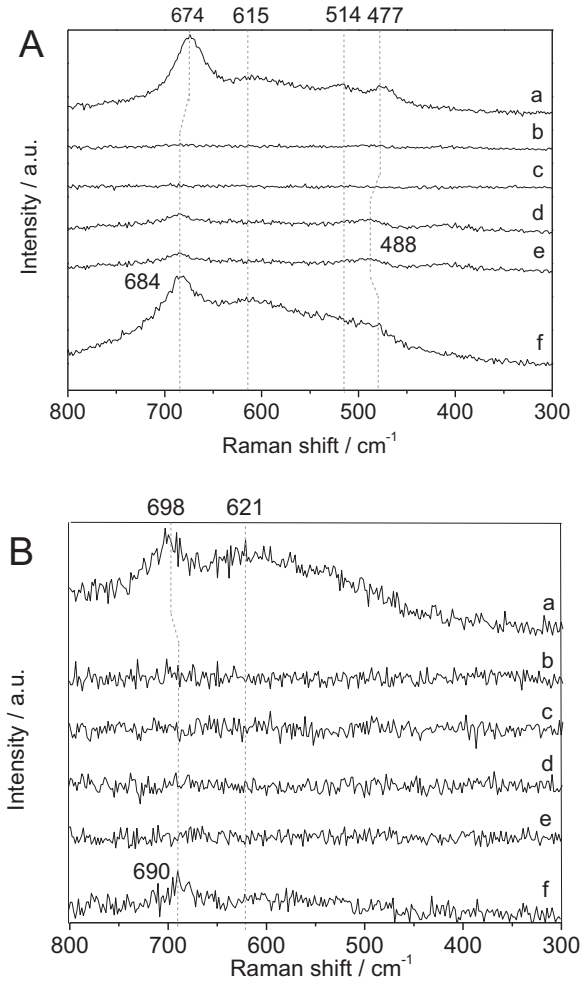

Fig. 7. *In situ* laser Raman spectra of Pt2Co (A) and 1.5K-Pt2Co (B) samples at different reaction stages: (a) before pretreatment; (b) after reduction by H_2 in water vapor; (c) 5 min reaction *in situ*; (d) 60 min reaction *in situ*; (e) 180 min reaction *in situ*; and (f) 2 min after reaction.

514, and 477 cm^{-1} were observed for Pt2Co, most likely assigned to Co_3O_4 in accordance with the results by Liorca et al. [37]. The catalyst of 1.5K-Pt2Co exhibited two bands at 698 and 621 cm^{-1}, suggesting that most of the Co species on the catalyst surface are Co_3O_4 according to the results by Hadjiev et al. [38]. These bands for Pt2Co and 1.5K-Pt2Co before pretreatment disappeared after pretreatment for 2 h, indicating that most of the Co oxides on the surface of the two catalyst coatings were reduced to zero-valence Co species. Interestingly, for Pt2Co, two weak bands at 684 and 488 cm^{-1}, which were assigned to CoO or Co_3O_4 [36,38], gradually appeared during the evolution of the PROX reaction. The intensities of the two bands were stable when the reaction time exceeded 1 h, indicating that metallic Co species on the catalyst surface are oxidized by O_2 in the feed stream within the initial reaction stage. In contrast to Pt2Co, no band was detected for the 1.5K-Pt2Co catalyst. As the two catalysts were exposed to air after the reaction, the bands approximately at 684 and 488 cm^{-1} were remarkably enhanced and broadened for Pt2Co. For 1.5K-Pt2Co, one band at 690 cm^{-1} was detected. This observation indicates that the metallic Co species present on the two catalyst surfaces during PROX were oxidized by air at room temperature. For Pt2Co, the *in situ* LRS demonstrated the co-existence of the metallic Co and its oxides during the PROX reaction. It can also be inferred that the redox equilibrium for Co can be achieved with the evolution of the reaction; however, this redox equilibrium appears to be negligible with the addition of K.

It should be pointed out that, under the same experimental conditions of *in situ* LRS measurement, the Raman spectra intensities of Pt2Co were roughly ten times those of 1.5K-Pt2Co. In Fig. 7, the scale of Raman intensity for Pt2Co is ten times that of 1.5K-PtCo, which could clearly demonstrate the changes in the two Raman spectra with the PROX reaction. Otherwise, the Raman spectra of 1.5K-Pt2Co seemed like a straight line if the same scale was taken as that of Pt2Co. Accordingly, the ratio of signal to noise of 1.5K-Pt2Co was lower than that of Pt2Co. We prepared a K_2O/Al_2O_3 catalyst coating with the solution of potassium nitrate (the K loading is the same as that of 1.5K-PtCo). No Raman reflection signal was found and K_2O is not Raman active. For 1.5K-Pt2Co, with the K addition, part of the Co species were likely covered by K_2O species, resulting in a significant decease in Raman spectra intensity.

3.2.3. XPS

The Pt2Co and 1.5K-Pt2Co were analyzed using XPS after the PROX reaction. The atomic ratio of Co in Pt_3Co, compared to the rest of the Co species on the catalyst surface (RCS), was determined to describe the portion of Pt_3Co on the catalyst coating. As all of the XPS spectra were generated under the same fitting method, the relative intensity ratio of Pt_3Co to the RCS peaks obtained represents

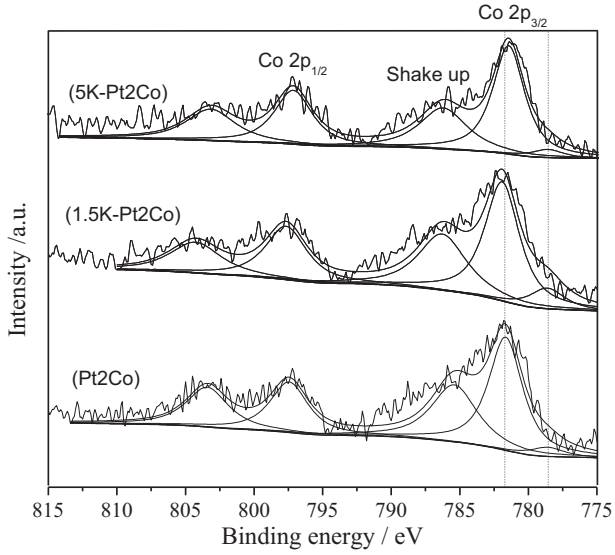

Fig. 8. Co 2p XPS spectra of after-reaction samples: Pt2Co, 1.5K-Pt2Co, and 5K-Pt2Co.

the relative content of the respective species [39]. As mentioned in Section 3.2.2, the metal Co species present on the catalyst surface during PROX are prone to oxidation by air after reaction, which reveals that the Co species are in an oxide state except for the Co in Pt_3Co (Fig. 7). The binding energy (BE) peaks were fitted at 778.6 eV as the Co $2p_{3/2}$ BE of Pt_3Co, which is 0.5 eV shift toward a higher BE compared with the metallic cobalt phase at 778.1 eV [40]. As the aim was to determine the amount of Pt_3Co on the surface of the catalyst coating, the other Co species were not differentiated during peak deconvolution.

The Co 2p photoelectron spectra recorded for the three coating samples are illustrated in Fig. 8. The XPS analytical results on the Co $2p_{3/2}$ BE are summarized in Table 2. A peak at approximately 781.6 eV for Co $2p_{3/2}$ was ascribed to both a Co surface phase (CSP) and Co oxide [41]. Strong shake-up satellites were clearly present, which are characteristic of CoO. Because the CoO, as opposed to Co_3O_4, has a strong shake-up satellite peak that is 5 eV higher than the main peak, as well as a spin-orbit coupling of approximately 15.5 eV [41]. These strong shake-up satellites definitively confirm the presence of CoO. The intensity of the peak at 778.6 eV (Pt_3Co), which is substantially lower than that at 781.6 eV, indicates that the predominance of the RCS is on the catalyst surface.

As presented in Table 2, 1.5K-Pt2Co showed the highest intensity ratio (0.17) of Pt_3Co to RCS ($IPt_3Co/IRCS$), roughly two times those of 0.08 and 0.07 for Pt2Co and 5K-Pt2Co, respectively. The intrinsic activity of Pt_3Co has proved to be higher than Pt at low temperatures [42]. The reason why Pt_3Co exhibits greater PROX activity is discussed in the following Section 3.2.5. It can be concluded that the highest catalytic activity of 1.5K-Pt2Co is attributed to the highest amount of Pt_3Co species in the catalyst surface region. In the case of 1.5K-Pt2Co, the unfavorable effect of the considerable increase in particle sizes (Figs. 5a and 6a) is overwhelmed by the promotional effect of the formation of Pt_3CO. The lowest $IPt_3Co/IRCS$ value of 0.07 among the three catalyst coatings was observed in Table 2 for 5K-Pt2Co. This can be explained by that an excessive K addition resulted in a coverage of K species on Pt species in the catalyst surface region. In comparison with Pt species, K species are less active if used solely as a catalyst. Thus, the inferior activity of 5K-Pt2Co to 1.5K-Pt2Co most likely results from the decreased Pt_3Co in the catalyst surface region.

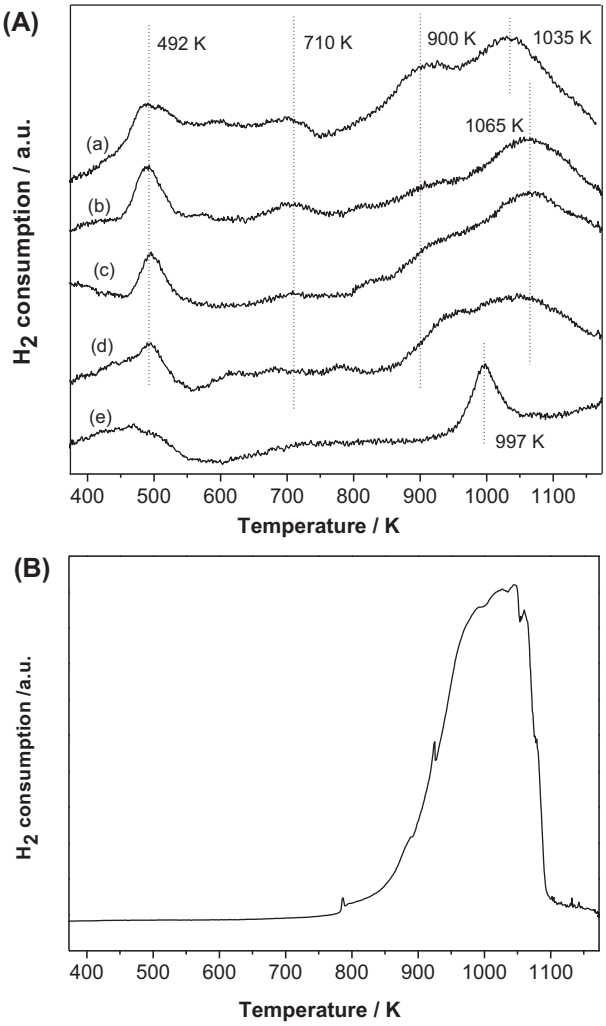

Fig. 9. (A) H_2-TPR profiles of (a) Pt2Co, (b) 1.5K-Pt2Co, (c) 3K-Pt2Co, (d) 5K-Pt2Co, and (e) 3K. (B) H_2-TPR profile of K_2O powder.

3.2.4. TPR

H_2-TPR tests were employed for the catalyst coatings as shown in Fig. 9(A). Several temperature regions of reduction were distinguished for the samples. The H_2 consumption in the reduction of the samples was calculated from the TCD signal after correction and calibration by the reduction results of standard CuO powders. This method was reported by Xia et al. [43]. The reduction of PtO_xCl_y, PtO_2 or oxygen shared with potassium was reported at *ca.* 492 K [44,45]. The H_2 consumptions of 100 mg sample at 492 K were measured as 0.016, 0,018, 0.016, and 0.011 m mol H_2 for Pt2Co, 1.5K-Pt2Co, 3K-Pt2Co, and 5K-Pt2Co, respectively. If the Pt ions for the above samples were all in the form of Pt^{+4} and could be completely reduced to metallic Pt, the theoretical H_2 consumption should be 0.0103 m mol H_2. The higher measured H_2 consumption than the theoretical one at 492 K indicates a possible existence of reduction of other species besides Pt. Arnoldy et al. reported that some partial reduction of Co^{3+} to Co^{2+} might take place below 515 K for CoO/Al_2O_3 [46]. The high H_2 consumption at 492 K most likely results from a partial reduction of Co species in this case. In accordance with the experimental results by Arnoldy et al. [46], the following detected reduction regions may be ascribed to reductions of Co species: the region at *ca.* 710 K corresponding to Co^{3+} ions in well-dispersed surface species, the region at *ca*, 900 K related to surface Co^{2+} ions, and those at *ca.* 1035–1065 K assigned to surface

Table 2
Cobalt $2p_{3/2}$ binding energies (BE) for different K to Pt ratios.

Sample	Co $2p_{3/2}$ BE				I_{Pt3Co}/I_{RCS} ($\times10^{-2}$)
	Pt_3Co BE (eV)	I_{Pt3Co}[a] ($\times10^2$) (CPS eV)	RCS BE (eV)	I_{RCS}[b] ($\times10^3$) (CPS eV)	
Pt2Co	778.6	6.8	781.6	8.6	8
1.5K-Pt2Co	778.6	15.9	781.9	9.1	17
5K-Pt2Co	778.6	5.77	781.5	7.6	7

[a] I_{Pt3Co} is the intensity (area) of Co $2p_{3/2}$ BE peak of Pt_3Co.
[b] I_{RCS} is the intensity (area) of Co $2p_{3/2}$ BE peak of RCS.

Co^{2+} or Co^{3+} ions occurring in diluted Co^{2+}-Al^{3+} spinel structures or in $CoAl_2O_4$.

To clarify the reduction of K species, a K_2O/Al_2O_3 catalyst coating of 3K was prepared with the same K loading of 3K-Pt2Co using the impregnation method as mentioned in section 2.1. As illustrated in Fig. 9 (A), a high reduction peak at *ca.* 997 K was detected. For the K-PtCo/Al_2O_3 catalyst coatings, this peak at 997 K was overlapped by the broad peak at 1065 K. A K_2O powder was prepared by the calcination of KNO_3 at 773 K and its TPR result is shown in Fig. 9 (B). The same peak at *ca.* 997 K was observed, which definitely verified the assignment of the peak at 997 K to the reduction of K species. This high reduction temperature at 997 K suggests that K exists in the form of non-reducible species on alumina for the K-PtCo/Al_2O_3 catalyst coatings during PROX considering the pretreatment temperature of 673 K in our case. Vordounis et al. [47] prepared sodium-doped specimens by dry impregnation of γ-alumina with aqueous solutions of $NaNO_3$ and determined that the addition of sodium to γ-alumina formed Al-O-Na bonds with a low sodium content. Thus, it can be conjectured that the potassium most likely formed Al-O-K bonds because K and Na are similar alkali metals. The Al-O-K bonds could reduce the interaction between the Pt or Co metallic particles and the alumina support. This weak interaction is favorable for the interaction of Pt and Co metallic species and can explain the favorable role of K in Pt_3Co formation for Pt-Co catalyst coatings.

3.2.5. DRIFT

DRIFT spectra of absorbed CO were measured for Pt2Co and 1.5K-Pt2Co. As shown in Fig. 10, Pt2Co and 1.5K-Pt2Co gave bands at 2066 and 2067 cm^{-1}, respectively, attributed to linear CO absorbed on Pt atoms [48]. No band at around 1850 cm^{-1} could be observed, which is assigned to bridged CO [49]. This absence of the bridged CO was also reported previously for intermetallic compounds of Pt_3Co, PtCu, Ni_3Sn, Ni_3Sn_2 and Ni_3Sn_4 on SiO_2 [42,50]. The absence can be explained by the proposal that the distance between adjacent Pt atoms on the surface of the Pt_3Co is greater than that on the surface of pure Pt [42]. This could be the evidence of the formation of Pt_3Co for Pt2Co and 1.5K-Pt2Co. Moreover, the intensity of the linear CO band for 1.5K-Pt2Co was obviously lower than that for Pt2Co. As presented in Table 2, 1.5K-Pt2Co exhibited the higher amount of Pt_3Co species than that of Pt2Co. It is suggested that absorption of CO is weakened by the Pt_3Co formation. The strong absorption of CO on Pt hinders the absorption of O_2, resulting in low PROX activity at low temperatures. Therefore, the formation of Pt_3Co on the catalyst surface is beneficial to the PROX reaction.

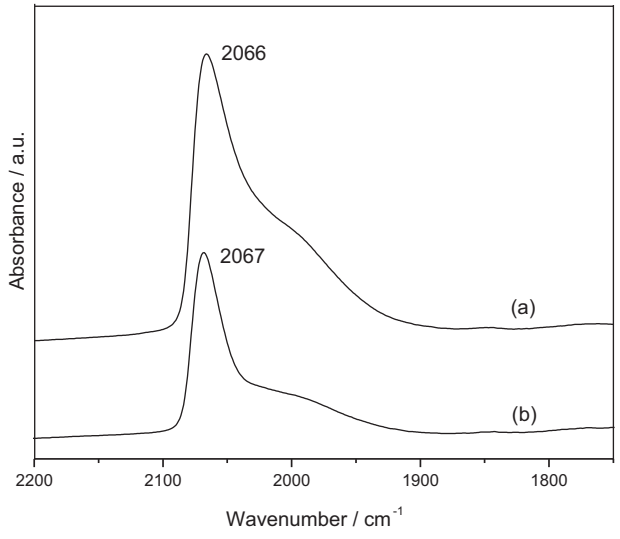

Fig. 10. DRIFT spectra of CO absorbed on (a) Pt2Co, and (b) 1.5K-PtCo.

In situ DRIFT spectra of Pt2Co and 1.5K-Pt2Co are shown in Fig. 11. In comparison with the CO absorption spectra in Fig. 10, red shifts were observed for the two catalysts with the evolution of the PROX reaction. The band at 2066 cm^{-1} for Pt2Co was shifted to 2041 cm^{-1}. For 1.5K-Pt2Co, the linear band at 2067 cm^{-1} was shifted down to 2065 and 2040 cm^{-1} with a broad shoulder at 1982 cm^{-1}. Xu et al. detected a similar red shift in the C–O stretch frequency at 423 K over a Pt/NaY zeolite catalyst [48]. In their experiments, a significant red shift of the C–O stretch frequency from H_2-free (2077 cm^{-1} at P_{CO} = 1.5 kPa to 2061 cm^{-1} at P_{CO} = 0.04 kPa) to H_2 rich gas (2054 cm^{-1} at P_{CO} = 1.5 kPa to 2049 cm^{-1} at P_{CO} = 0.04 kPa) was observed. Those experiments suggested that the shift of the C–O stretch frequency resulted from a H_{ad}-induced lowering of the CO_{ad} coverage and from a modification of the Pt–CO bond because of the interaction with the co-adsorbed H_{ad} species. The hydrogen adsorption leads to a weakening of the Pt–CO interaction. Hence, in our cases, the remarkable red shifts indicate a similarly weakened Pt-CO interaction because of the co-adsorption of CO and H_2 over Pt atoms during the PROX reaction. The shoulder at 1982 cm^{-1} likely results from CO bound to Pt atoms with a coordination number close to 3 or less [51] or a cluster consisting of less than 5 atoms [52].

It should be noted that a band at 2112 cm^{-1} gradually appeared with the evolution of the PROX reaction for Pt2Co (Fig. 11 A), which corresponds to Co^{x+}-CO (Co^{x+} indicates the Co species in different oxidation sates)[53]. *In situ* laser Raman spectra of Pt2Co (Fig. 7A) definitively confirmed the co-existence of the metallic Co and its oxides during the PROX reaction. By correlating the DRIFT and Raman results of Pt2Co, we propose that the reduced metallic Co of RCS reacted with O_2 in the gas phase and turned into Co^{x+} for the Pt2Co catalyst. Subsequently, the Co oxides reacted with the absorbed CO, which produced CO_2 and reduced the Co^{x+} to metallic Co.

In contrast to Pt2Co, no band in the range 2100–2180 cm^{-1} was observed for the 1.5K-Pt2Co catalyst during the PROX reaction (Fig. 11B), indicating that CO was mainly adsorbed on the metallic Pt and Co. This result is in good agreement with the LRS of 1.5K-Pt2Co (Fig. 7B), which indicated the nonexistence of a redox equilibrium as shown by Pt2Co. This is most likely because the increased amount of the Pt_3Co intermetallic compound in the catalyst surface region, as shown in Fig. 8 and Table 2, resulted in less Co species of RCS available for the redox mechanism.

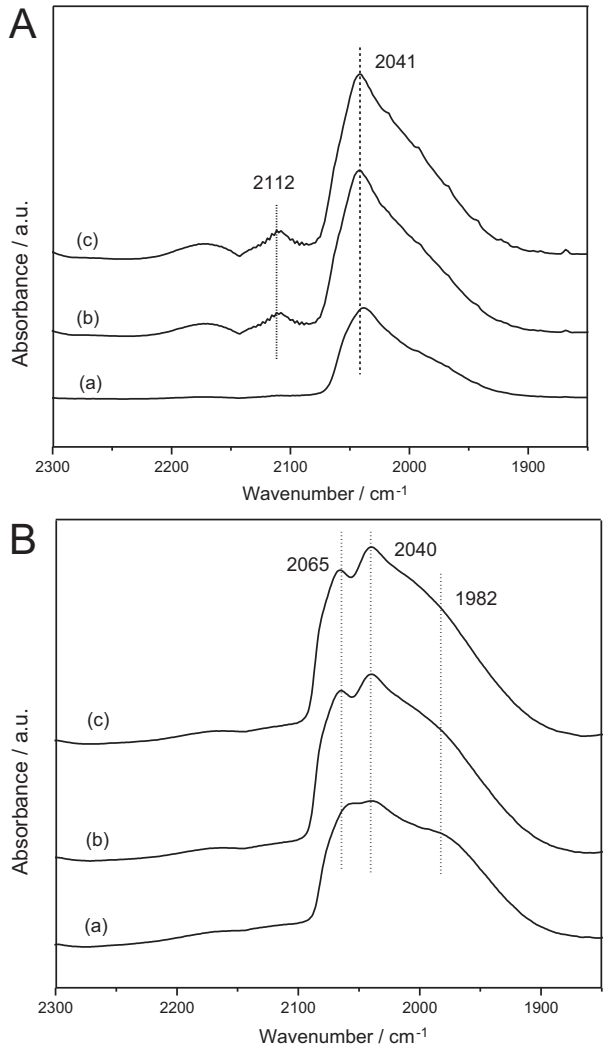

Fig. 11. *In situ* DRIFT spectra of Pt2Co (A) and 1.5K-Pt2Co (B): (a) 5 min reaction *in situ*; (b) 60 min reaction *in situ*; (c) 180 min reaction *in situ*.

The existence of the redox equilibrium for Co during PROX is desirable to this reaction. 1.5K-Pt2Co showed the highest catalytic activity among all catalysts but, in turns, eliminated the redox equilibrium observed for the catalyst without K. As seen in Fig. 7A, for Pt2Co, when the reaction time exceeded 1 h, the gradually stabilized intensities at 684 and 488 cm^{-1} (assigned to Co oxides) were remarkably lower than those of the sample exposed to air after the reaction, indicating that only a small part of metallic Co species were involved in the redox equilibrium for Co. The contribution of the redox equilibrium for Co to the PROX seems not remarkable. Both the redox equilibrium and Pt_3Co formation are beneficial for PROX, and 1.5K-Pt2Co exhibited the highest amount of Pt_3Co species in the catalyst surface region. Therefore, the superiority of 1.5K-Pt2Co to Pt2Co can be probably explained by that the unfavorable effect of the elimination of redox equilibrium for Co is overwhelmed by the favorable effect of an increase in the Pt_3Co formation. As shown in Fig. 2, 1.5K-Pt2Co exhibited a higher catalytic activity than 1.5K-Pt. Masatoshi et al. [29] reported that, for K-Pt/Al_2O_3 catalysts, potassium weakened the interaction between CO and Pt by changing the adsorption sites. For the lower catalytic activity of 1.5K-Pt than that of 1.5K-Pt2Co, one of the possible explanations is that the potassium of 1.5K-Pt contributes less to the weakness of the interaction between CO and Pt than the Pt_3Co of 1.5K-Pt2Co. Further investigations are needed to clarify and verify this explanation.

4. Conclusions

This study investigated the catalytic performance and characterization of K-PtCo/Al_2O_3 catalyst coatings for the PROX reaction in a micro-reactor. The addition of potassium can enhance the catalytic activities at low temperatures and can widen the window of operation in terms of reaction temperatures, thus exhibiting easy reaction control and lower energy consumption for its application. The most active catalyst coating of 1.5K-Pt2Co (with a low Pt loading of 1 wt%) can decrease CO concentrations from 1% to a value of less than 10 ppm at a high *GHSV* of 120,000 ml g^{-1} h^{-1} in a temperature range 393–433 K. TEM, HRTEM and XPS characterizations showed that a small amount of K (K/Pt molar ratio = 1.5) could definitively promote Pt_3Co formation, coinciding with an increase in the average particle size. The Pt_3Co formation is beneficial and crucial to the PROX reaction. The highest catalytic activity of 1.5K-Pt2Co is attributed to the highest amount of Pt_3Co species in the catalyst surface region. For PtCo/Al_2O_3 catalyst coatings, redox equilibrium for Co was observed during PROX. In contrast, with the addition of K, this redox equilibrium disappeared, most likely because of the increased amount of Pt_3Co phase in the catalyst surface region.

Acknowledgements

This study was financially supported by the China Natural Science Foundation (Contract No. 21176069), Program for New Century Excellent Talents in University (NCET-10-0380) and the Fundamental Research Funds for the Central Universities (WG1213011).

References

[1] I. Rossetti, C. Biffi, C.L. Bianchi, V. Nichele, M. Signoretto, F. Menegazzo, E. Finocchio, G. Ramis, A.D. Michele, Applied Catalysis B: Environmental 117–118 (2012) 384–396.
[2] Z. Zhao, X. Lin, R. Jin, G. Wang, T. Muhammad, Applied Catalysis B: Environmental 115–116 (2012) 53–62.
[3] O.H. Laguna, M.A. Centeno, M. Boutonnet, J.A. Odriozola, Applied Catalysis B: Environmental 106 (2011) 621–629.
[4] P. Panagiotopoulou, D.I. Kondarides, X.E. Verykios, Catalysis Today 181 (2012) 138–147.
[5] E.D. Park, D. Lee, H.C. Lee, Catalysis Today 139 (2009) 280–290.
[6] C. Galletti, S. Specchia, G. Saracco, V. Specchia, Chemical Engineering Science 65 (2010) 590–596.
[7] S.K. Jain, E.M. Crabb, L.E. Smart, D. Thompsett, A.M. Steele, Applied Catalysis B: Environmental 89 (2009) 349–355.
[8] F. Mariño, C. Descorme, D. Duprez, Applied Catalysis B: Environmental 54 (2004) 59–66.
[9] S.Y. Chin, O.S. Alexeev, M.D. Amiridis, Journal of Catalysis 243 (2006) 329–339.
[10] J. Xu, P. Li, X. Song, Z. Qi, J. Yu, W. Yuan, Y.-F. Han, Industrial and Engineering Chemistry Research 49 (2010) 4149–4155.
[11] Y.-F. Han, M.J. Kahlich, M. Kinne, R.J. Behm, Applied Catalysis B: Environmental 50 (2004) 209–218.
[12] Y. Huang, A. Wang, X. Wang, T. Zhang, International Journal of Hydrogen Energy 32 (2007) 3880–3886.
[13] J. Choi, C.B. Shin, D.J. Suh, Catalysis Communications 9 (2008) 880–885.
[14] S. Guerrero, J.T. Miller, A.J. Kropf, E.E. Wolf, Applied Catalysis A: General 328 (2007) 27–34.
[15] C.S. Polster, R. Zhang, M.T. Cyb, J.T. Miller, C.D. Baertsch, Journal of Catalysis 273 (2010) 50–58.
[16] J. Xu, T. White, P. Li, C. He, J. Yu, W. Yuan, Y.-F. Han, Journal of the American Chemical Society 132 (2010) 10398–10406.
[17] C. Dupont, F. Delbecq, D. Loffreda, Y. Jugnet, Journal of Catalysis 278 (2011) 239–245.
[18] X. Yu, S.-T. Tu, Z. Wang, Y. Qi, Chemical Engineering Journal 116 (2006) 123–132.
[19] X. Yu, S.-T. Tu, Z. Wang, Y. Qi, Journal of Power Sources 150 (2005) 57–66.
[20] S. Specchia, V. Specchia, Industrial and Engineering Chemistry Research 49 (2010) 6803–6809.
[21] G. Kolb, J. Schürer, D. Tiemann, M. Wichert, R. Zapf, V. Hessel, H. Löwe, Journal of Power Sources 171 (2007) 198–204.

[22] S.-M. Hwang, O.J. Kwon, S.H. Ahn, J.J. Kim, Chemical Engineering Journal 146 (2009) 105–111.
[23] G. Chen, Q. Yuan, H. Li, S. Li, Chemical Engineering Journal 101 (2004) 101–106.
[24] C. Galletti, S. Specchia, G. Saracco, V. Specchia, Chemical Engineering Journal 154 (2009) 246–250.
[25] P.V. Snytnikov, M.M. Popova, Y. Men, E.V. Rebrov, G. Kolb, V. Hessel, J.C. Schouten, V.A. Sobyanin, Applied Catalysis A: General 350 (2008) 53–62.
[26] N. Maeda, T. Matsushima, H. Uchida, H. Yamashita, M. Watanabe, Applied Catalysis A: General 341 (2008) 93–97.
[27] K.-Y. Kim, S.W. Nam, J. Han, S.P. Yoon, T.-H. Lim, H.-I. Lee, Journal of Industrial and Engineering Chemistry 14 (2008) 853–859.
[28] H. Li, X. Yu, S.-T. Tu, J. Yan, Z. Wang, Applied Catalysis A: General 387 (2010) 215–223.
[29] M. Kuriyama, H. Tanaka, S. Ito, T. Kubota, T. Miyao, S. Naito, K. Tomishige, K. Kunimori, Journal of Catalysis 252 (2007) 39–48.
[30] C. Kwak, T.-J. Park, D.J. Suh, Applied Catalysis A: General 278 (2005) 181–186.
[31] X. Yu, H. Li, S.-T. Tu, J. Yan, Z. Wang, International Journal of Hydrogen Energy 36 (2011) 3778–3788.
[32] M. Echigo, N. Shinke, S. Takami, T. Tabata, Journal of Power Sources 132 (2004) 29–35.
[33] T. Suetsuna, S. Suenaga, T. Fukasawa, Applied Catalysis A: General 276 (2004) 275–279.
[34] I.H. Son, M. Shamsuzzoha, A.M. Lane, Journal of Catalysis 210 (2002) 460–465.
[35] T. Xiao, S. Ji, H. Wang, K.S. Coleman, M.L.H. Green, Journal of Molecular Catalysis A: Chemical 175 (2001) 111–123.
[36] M.A. Vuurman, D.J. Stufkens, A. Oskam, G. Deo, I.E. Wachs, Journal of the Chemical Society, Faraday Transactions 92 (1996) 3259–3265.
[37] J. Llorca, P. Piscina, J.-A. Dalmon, N. Homs, Chemistry of Materials 16 (2004) 3573–3578.
[38] V.G. Hadjiev, M.N. Iliev, I.V. Vergilov, Journal of Physics C: Solid State Physics 21 (1988) 199–201.
[39] Y. Zhang, H. Xiong, Kong. Liew, J. Li, Journal of Molecular Catalysis A: Chemical 237 (2005) 172–181.
[40] U. Bardi, B.C. Beard, P.N. Ross, Journal of Catalysis 124 (1990) 22–29.
[41] Z. Zsoldos, L. Guczi, Journal of Physical Chemistry 96 (1992) 9393–9400.
[42] T. Komatsu, A. Tamura, Journal of Catalysis 258 (2008) 306–314.
[43] S. Xia, Z. Yuan, L. Wang, P. Chen, Z. Hou, Applied Catalysis A: General 403 (2011) 173–182.
[44] H. Lieske, G. Lietz, H. Spindler, J. Völter, Journal of Catalysis 81 (1983) 8–16.
[45] H.C. Yao, M. Sieg, H.K. Plummer Jr., Journal of Catalysis 59 (1979) 365–374.
[46] P. Arnoldy, J.A. Moulijn, Journal of Catalysis 93 (1985) 38–54.
[47] L. Vordounis, P.G. Koutsoukos, A. Lycourghiotis, Journal of Catalysis 98 (1986) 296–307.
[48] J. Xu, X.-C. Xu, L. Ouyang, X.-J. Yang, W. Mao, J. Su, Y.-F. Han, Journal of Catalysis 287 (2011) 114–123.
[49] M.J. Dees, T. Shido, Y. Iwasawa, V. Ponec, Journal of Catalysis 124 (1990) 530–540.
[50] A. Onda, T. Komatsu, T. Yashima, Journal of Catalysis 221 (2003) 378–385.
[51] M.J. Kappers, J.H. van der Maas, Catalysis Letters 10 (1991) 365–372.
[52] A.L. Ankudinov, J.J. Rehr, J.J. Low, S.R. Bare, Journal of Chemical Physics 116 (2002) 1911–1919.
[53] J. Jansson, Journal of Catalysis 194 (2000) 55–60.